Q. J. R. Meteorol. Soc. (2006), **999**, pp. 1–999 doi: 10.1256/qj.06.?

Why the West Wind Wobbles: Viewing Annular Modes as Stochastically-Excited Potential Vorticity Reservoirs

By Jason C. Goodman[1]* and Arnaud Czaja[2]
[1]*Department of Physical Oceanography, Woods Hole Oceanographic Institution, Woods Hole, MA*
[2]*Department of Physics, Imperial College, London UK*

Draft version for February 1, 2006

SUMMARY

The Northern and Southern Annular Modes can be thought of as modulating the polar pools of high potential vorticity (PV). Meridional PV fluxes caused by synoptic weather stochastically add or remove PV from this reservoir, gradually increasing or decreasing the strength of the annular mode. We demonstrate that much of the variability of the annular modes in both a 3-layer quasigeostrophic model and in NCEP-NCAR reanalyses can be explained by this simple stochastic process.

1. INTRODUCTION

The Northern and Southern Annular Modes (NAM/SAM) are the leading modes of variability in their respective hemispheres (*Thompson and Wallace*, 2000a) and represent a change in the strength and latitude of the mid-latitude westerly wind. The NAM/SAM also go by the names "Arctic/ Antarctic Oscillation" and are rooted in the older idea of a "Zonal Index" (*Rossby and Willett*, 1948; *Namias*, 1950) describing vacillations from a zonally-symmetric point of view. The time sequence of high and low phases of the annular modes have been linked to major climate signals, including recent trends in surface temperature (*Thompson and Wallace*, 2000a,b). This motivates the search for a firm understanding of their dynamics.

As emphasized recently in the review by (*Thompson et al.*, 2003), it is clear that the annular modes essentially reflect interactions between transient eddies and the midlatitude westerly winds. These interactions are believed to set the timescale (about 10 days) and the spatial pattern of the annular modes (e.g., *Feldstein*, 2000; *Lorenz and Hartmann*, 2001, 2003). Building upon this view, *Vallis et al.* (2004) recently designed an illustrative model of annular mode variability: stirring of potential vorticity by baroclinic eddies in a localized latitude band tends to induce annular zonal wind anomalies, and the system's inherent time integration of eddy forcing leads to a long decorrelation timescale for the zonal wind anomalies. The potential vorticity (PV) view of the annular modes put forward by *Vallis et al.* (2004) in an idealized context (see also the observational study by *Hartmann* (1995)) is very appealing because it reduces the dynamics of the annular modes to that of a tracer, namely the PV.

We wish to apply this PV framework to both fairly-realistic models and real-world observations by proposing that annular mode variability merely reflects changes in the amount of PV stored in high latitudes reservoirs or "PV pools". To illustrate fluctuations in the "PV pool", we present Figure 1, which shows the potential vorticity anomaly associated with the NAM at 200 mbar, for the quasigeostrophic model discussed in Section 2(*a*). A polar positive center of action is clearly seen, surrounded by a mid-latitude negative center (and a tropical positive center). The subpolar zero-PV-anomaly contour is roughly aligned with the 55° latitude line. Synoptic weather events carry potential vorticity across this boundary. The amount of PV in the pool, i.e. in our view, the annular mode, thus varies as a time-integrated response to stochastic PV fluxes through the boundary.

This work bridges the gap between analytical models and idealized simulations on the one hand, and purely statistical correlation-and-regression work using real-world data on the other hand. We build our simple stochastic model from a fairly rigorous foundation in Section 3, and test it against model and real-world data in Section 4. In section 5 we discuss the issue of eddy mean flow feedbacks from the PV reservoir perspective, while in section 6 we discuss further tangential issues. We conclude in section 7 with a summary of our main results.

2. MODELS AND DATA

(*a*) *3-layer quasigeostrophic model*

Section 4(*a*) uses output from a 3-layer quasigeostrophic potential vorticity model, based on a model by *Molteni* (1994). This model is constructed in spherical coordinates at T21 spectral resolution (about 5° spatial resolution), with realistic (albeit coarse) topography, bottom drag, and radiative damping dissipation. A steady potential vorticity input forcing is applied, whose spatial pattern is chosen empirically to ensure that the model's climatology is quite close to the observed climatology for for December-March of 1983-1993. The model is run in "perpetual winter" conditions. For full details see *Molteni* (1994).

We define "the model's northern annular mode" (mNAM) as the leading empirical orthogonal function (*North*, 1984) of the model's streamfunction output in spectral coordinates over the entire globe and at all three levels, and display the resulting pattern and timeseries in Figure 2. *Goodman and Marshall* (2003) have previously discussed the connection of this pattern to the model's nearly-stationary "neutral vector" states. Note the strong autocorrelation and persistence of the mNAM timeseries. The last 4850 daily fields from a 5000-day model run were used in the EOF analysis and in the timeseries analysis discussed in Section 4(*a*).

* Corresponding author: Department of Physical Oceanography, Woods Hole Oceanographic Institution, Woods Hole, MA 02543, USA. E-mail: <*jgoodman@whoi.edu*>

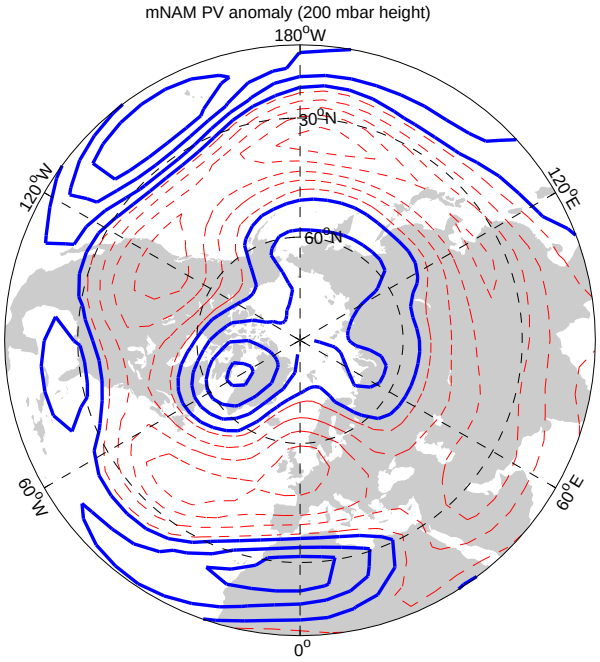

Figure 1. Quasi-geostrophic potential vorticity anomaly at 200 mbar, associated with a unit perturbation of the NAM pattern in a 3-layer quasigeostrophic model (see Figure 2). Contour interval $2.5{\cdot}10^{-6}\mathrm{s}^{-1}$; thick solid (thin dashed) lines indicate positive (negative) perturbations.

We also produced timeseries of the time-varying potential vorticity flux through each latitude line in the model's gridded output, at each vertical level, by integrating $q \cdot v$ around each latitude circle and subtracting away the time-mean flux at each latitude and level. These data will be used in Section 4(*a*) to test the autoregressive "reservoir" model developed in Section 3.

(*b*) *NCEP-NCAR data*

Section 4(*b*) uses NCEP-NCAR reanalysis data (*Kalnay et al.*, 1996) over the period 1995-2004. The data consist of daily outputs on a 2.5°$\times$ 2.5° grid, at 17 pressure levels.

Daily values of the Northern Annular Mode / Arctic Oscillation (NAM, aka AO) and Southern Annular Mode (SAM) were obtained from the NOAA Climate Prediction Center†. The NAM pattern is defined as the leading EOF of monthly 1000-mb height anomalies north of 20°, and similarly but at 700 mb for the SAM in the southern hemisphere. The NAM/SAM indices represent the projection of daily geopotential timeseries onto these patterns. We use daily NAM index data between December and February (inclusive) for 1995-2004 (where Dec 1994-Feb 1995 is "winter 1995", and so on), and June-August (inclusive) of the same years for SAM. The NAM/SAM patterns and timeseries are shown in Figures 3 and 4.

3. AUTOREGRESSIVE MODEL DERIVATION

In mathematical terms, our model takes a very simple form. We begin with a statement of conservation of potential vorticity q following the flow, except for a linear damping of strength λ and a constant forcing f_q:

$$\frac{Dq}{Dt} = -\lambda q + f_q$$

We integrate this term over the polar region bounded by a closed boundary P (but postpone the choice of P for now)

$$\frac{\partial Q}{\partial t} = \oint_P vq dl - \lambda Q + F_q \tag{1}$$

† http://www.cpc.ncep.noaa.gov/products/precip/CWlink/ENSO/verf/new.teleconnections.shtml

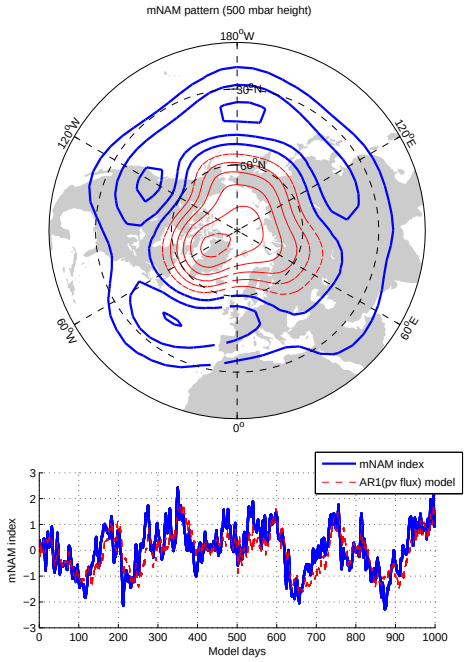

Figure 2. The "model north annular mode" (mNAM), the 3-layer quasi-geostrophic model's leading mode of daily variability (first EOF). Upper panel: mNAM structure (geopotential height anomaly at 500 mbar). Contour interval 30 m; thick solid (thin dashed) contours indicate positive (negative) anomalies. Lower panel: Amplitude of mNAM pattern over time (thick solid line). 1000 of 4850 analyzed days are shown. Thin dashed line: output of the autoregressive PV flux model discussed in Sections 3 and 4(*a*). The vertical lines indicate the time span of each winter.

where capitalized quantities now represent area integrals over the domain enclosed by the boundary P. We have used the divergence theorem and an assumption of 2-D incompressible flow to replace the PV advection part of DQ/DT with a boundary integral of PV flux through P. v is the component of velocity normal to P (the meridional wind, if P is chosen as a latitude circle), and dl is a differential path segment.

We propose that the annular modes can be thought of as a weighted vertical integral or sum of variations in Q through the troposphere, for some appropriately-chosen P. That is,

$$AM = \int b(p) Q' dp$$

where AM is the annular mode index, b is a vertical weighting function to be determined, and primed terms represent deviations from the time-mean. Integrating (1) vertically and taking its time-varying part, hence removing the constant forcing f_q:

$$\frac{\partial AM}{\partial t} = \int b \oint_P (vq)' dl dp - \lambda \cdot AM$$

$$\frac{\partial AM}{\partial t} = \int bQV dp - \lambda \cdot AM$$

where $QV(p) = \oint_P (vq)' dl$ represents the time-varying part of the PV flux through P at each vertical level.

I *Discretization*

In practice, our available data consists of daily sampled output from either the 3-layer QG model or NCEP-NCAR analysis, and is available at fixed vertical levels. We discretize the equations in time and pressure, forming a lag-one autoregressive (AR1) difference equation:

$$AM(n) = (1-\lambda) AM(n-1) + \mathbf{b} \cdot \mathbf{QV}(n-1) \tag{2}$$

where we have redefined $\mathbf{b}$ and λ to subsume the timestep term Δt =1 day. $\mathbf{b}$ and $\mathbf{QV}$ are now vectors, with one element for each vertical level at which data is available.

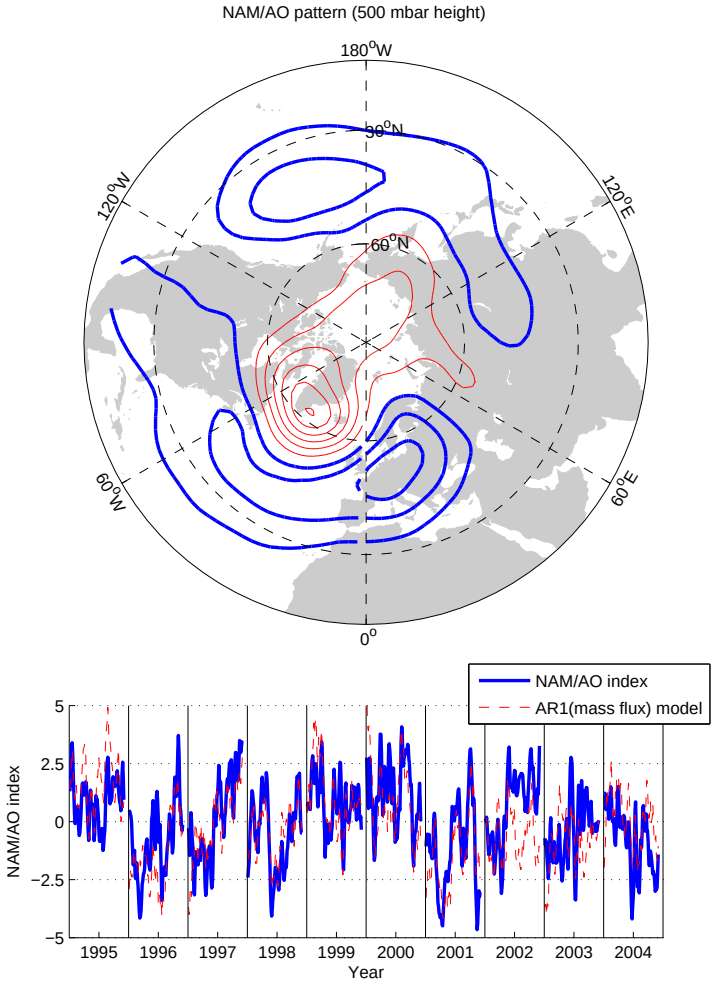

Figure 3. Same as Figure 2, but showing the "north annular mode", the leading mode of variability of monthly northern-hemisphere NCEP-NCAR data. As before, upper panel: NAM structure, contour interval 15 m; lower panel: NAM amplitude over time (thick solid line), for Dec-Feb, 1995-2004. Thin dashed line indicates output of the autoregressive mass-flux model discussed in Sections 3 and 4(*b*).

We now have a very simple model for AM variability. Because PV is conserved, the annular mode persists from one day to the next apart from a small damping effect, and is stochastically excited by eddy-driven PV fluxes into the polar zone. Let's test this model: how much AM variability can it explain?

4. TESTING THE AUTOREGRESSIVE MODEL

(*a*) *3-layer QG Model*

To test our autoregressive model, we perform a least-squares analysis on daily data to identify the values of λ, $\mathbf{b}$, and the initial condition $AM(n=0)$ which provide the best fit between the true annular mode index and the autoregressive model's output‡. We use

‡ The AR1 model fitting was performed using the `arx()` function of the System Identification Toolbox in Mathworks' MATLAB package

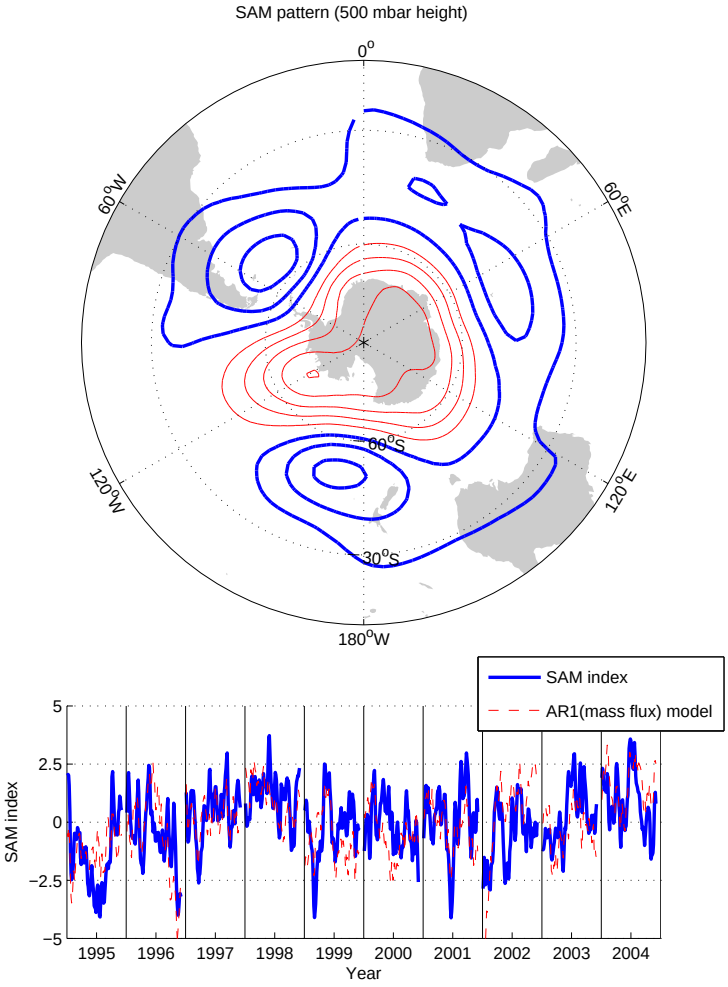

Figure 4. Same as Figures 2 and 3, but showing the "south annular mode", the leading mode of variability of monthly southern-hemisphere NCEP-NCAR data.

the correlation between AR1 output and the true index to gauge the model's skill. While we treat λ and $\mathbf{b}$ as free parameters, we will check *a posteriori* that they have physically-sensible values.

Figure 1 shows an apparent boundary between polar and subtropical PV pools at 55° N, so we set the boundary P at the nearest model gridpoint, 58° N, as a first guess.

We find that a best-fit AR1 model forced by PV fluxes through 58° N has a correlation of 0.86 with the mNAM timeseries. Remember that while the mNAM data was used to find the best-fit λ and 3-element vector $\mathbf{b}$, the AR(1) timeseries uses only these four fixed parameters and the QV(58) timeseries at three different heights to "predict" mNAM. Figure 2 shows a comparison of the mNAM timeseries and the output of the AR1 model.

The correlation suffices to describe the similarity of the AR1 output to the mNAM timeseries. There is no need to compare the timeseries amplitudes because since the AR1 model is linear, one can ensure that the overall variances match exactly by rescaling the $\mathbf{b}$ vector.

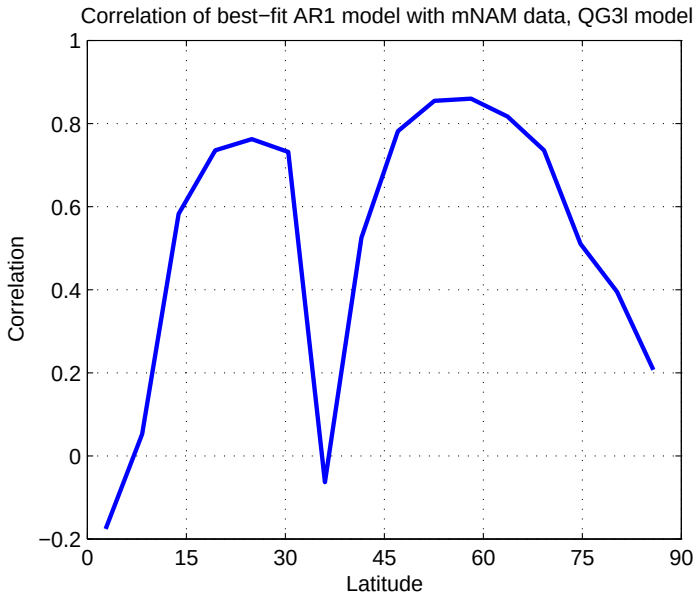

Figure 5. Correlation between the 3-layer model's north annular mode (mNAM) index and the output of a best-fit lag-1 autoregressive model. Autoregressive model is driven by potential vorticity flux through a single latitude line; correlation is plotted as a function of latitude choice.

The $\mathbf{b}$ vector has values of [0.72,0.52,.45] at pressure levels [200,500,800] mb.§ The sign is such that positive PV flux into the polar zone tends to strengthen the positive PV anomaly there and cause a positive AO tendency, as one would expect. Note that in the mean the PV fluxes are equatorward (e.g., *Held and Schneider*, 1999) so that a positive phase of the annular mode (higher PV in the polar pool) reflects less export of PV from high to low latitudes than on average. The similar values at the three levels suggest that PV flux at all levels are effective in driving the mNAM. The best-fit value of λ is 1/31 days. This is similar to the 25-day timescale for parameterized temperature relaxation in the model, but the connection between λ and temperature relaxation is not simple: See Section 6(*b*).

We picked latitude 58° N as our boundary *a priori*, based on the mNAM pattern. Could one do as well or better by picking another latitude? In Figure 5, we consider every possible choice of latitude, and generate separate best-fit AR1 models driven by PV fluxes through each latitude line. We plot the correlation between the AR1 model output and the true mNAM as a function of the latitude choice. Our *a priori* choice is in fact the best choice one could make.

Note the secondary maximum in the AR1 model fit at around 25° N. This is explained by noting that the mNAM PV pattern has one center of action over the pole, as previously discussed, but also a secondary maximum at around 35°. PV flux into the subtropical box from further south, at around 25° N, can also exert a stochastic control on the mNAM. Thus, we could more precisely describe the mNAM as a *two-reservoir* system, in which both PV flux from the subtropical to the polar reservoir, and into the subtropical reservoir from the tropics, are important. As one would expect, the sign of the sensitivity vector $\mathbf{b}$ is reversed for the AR1 model based on 25° fluxes as compared to 58°. One might also expect that an AR1 model fit to the mNAM using PV fluxes at *both* 25 and 58° might give an even better fit. We find the gain to be modest (correlation of 0.90 as opposed to 0.86), considering that this doubles the number of free parameters to be fit.

(*b*) *NCEP-NCAR Reanalysis Data*

The PV to investigate in the observations is Ertel's potential vorticity (*Gill*, 1982), not simply the QG approximation considered in the previous section. As a simple proxy for its associated meridional fluxes, we have computed the meridional mass fluxes within isentropic layers, also known as thickness fluxes. The relationship of the latter to Ertel's PV can be understood by considering the potential vorticity q of a shallow layer of air contained between two isentropes,

$$q = \frac{f + \zeta}{h}$$

where f is the planetary vorticity, ζ is relative vorticity, and h is the thickness between the two isentropes. If variations in h are small ($h = h_0 + h'(t)$, with $h' << h_0$) then to first order in time perturbations, we have

$$q' \simeq \frac{\zeta'}{h_0} - \frac{f h'}{h_0^2}$$

§ We normalize all $\mathbf{b}$ vectors to unit magnitude in this work for ease of comparison, and because their units are awkward.

For length scales larger than the deformation radius $\sqrt{gh_o}/f$ where g is gravity, the relative vorticity contribution to q' can be neglected so that PV fluctuations are proportional to isentropic thickness fluctuations, with the opposite sign

$$v'q' \simeq -f\frac{v'h'}{h_0^2}$$

This "long wave" approximation to the PV certainly filters some of the high frequency synoptic PV fluxes. As will be seen however, a surprisingly large amount of annular mode variability is still captured by this simpler PV flux forcing.

At each grid point, the meridional mass flux within pressure levels was interpolated on a finer pressure grid (10mb resolution) then partitioned into a predetermined set of isentropic layers. The latter have a resolution of 5K (other choices were tested and the results are not particularly sensitive to this choice). Figure 6 shows the isentropic layers for Northern and Southern Hemisphere winters of 2003. For each day, the meridional mass fluxes within isentropic layers were subsequently averaged along latitude circles to provide the basic isentropic mass flux $MV(\theta, t)$ expressed in units of 10^9 kg s^{-1} per 5 K. Note that daily surface pressure maps were used to remove those isentropic layers 'below' the ground. An indication of which they might be is provided by the gray lines in Figure 6.

We drive our AR1 model using mass fluxes along a range of isentropes spanning the bulk of the troposphere: We use 238-293 K at 80 S; 288-343 K at 20 S; 288-363 K at 20 N, and 238-313 K 80 N, with smoothly-varying transitions between these points. Note that we include some isentropes colder than the time-mean surface isotherm. Also, for statistical consistency, we choose the same isentrope span $\Delta\theta$ for each latitude line in a given hemisphere ($\Delta\theta = 55$ K in the south, $\Delta\theta = 75$ K in the north).

I *Statistical Tests*

In section 4(*a*), our autoregressive model fit five free parameters (λ, the three elements of $\mathbf{b}$, and an initial condition) to 4850 daily observations of the mNAM. With such a highly overconstrained system and an excellent fit, the statistical significance of the result was not in doubt.

For the NCEP-NCAR data, however, we have 13-16 free parameters (The $\mathbf{b}$ vector has one element for each isentrope used as input data) and only 920 daily values of the NAM and SAM. Even worse, the annular mode timeseries have very high lag-autocorrelations, so the number of independent observations is much smaller. We need a way to gauge the significance of our results.

Thus, we compare the performance of AR1 models based on the true isentropic mass-flux data MV to the performance of AR1 models based on synthetic, random inputs. The synthetic data is randomly generated, then filtered to ensure it has the same variance, lag-autocorrelation, and inter-isentrope covariance pattern as MV – but no connection to the annular mode index. The mean correlation of 100 AR1 models based on synthetic data with the true NAM/SAM index gives an indication of how good a fit may be expected to occur by chance alone; we also show the line below which 95% of the synthetic correlations lie.

To further reduce the chance of spurious fits to the data, we use a "jackknife" sampling technique. We withhold one year of data, using the other nine to compute the best-fit AR1 model, and then test the model by computing the correlation of its output over the course of the withheld year. We repeat this process withholding each year in turn; our goodness-of-fit measure is the average correlation over all ten jackknife repetitions.

II *Southern Annular Mode*

Figure 7 shows the AR1 model's correlation to the SAM, using NCEP isentropic mass-flux data as input. The result is strikingly similar to Figure 5: The SAM is highly responsive to mass fluxes at 60° and, to a lesser extent, 22.5°. The $60^\circ S$ latitude is also consistent with the latitude at which the SAM Ertel's PV anomaly vanishes in Hartmann's 1995 observational study. Thus, as with the mNAM, meridional fluxes of PV are most effective at driving the annular mode when they occur through the boundary of the PV reservoirs.

The lower panel of Figure 4 shows the agreement between the autoregressive model's output and the observed SAM index, using mass fluxes at 62° S, the best possible choice. The damping/persistence parameter λ is 1/28 days for this choice.

If we construct an AR1 model driven by mass fluxes through *both* 60° and 25°, the model fit improves a moderate amount, to 0.65.

III *Northern Annular Mode*

Figure 7 shows the AR1 model's correlation to the AO / NAM, using NCEP mass fluxes as input. Once again, we see a characteristic two-humped curve: The SAM is highly responsive to mass fluxes at 55° and 30°. It may seem a bit odd that the correlation is significant well into the polar zone (70-80 N). This is probably because the mass fluxes have a strong spatial correlation due to the size of the synoptic eddies; a storm which moves mass through 70 N is usually also moving mass through 55 N. As before, the lower panel of Figure 3 shows the agreement between the autoregressive model's output and the observed AO / NAM index, using mass fluxes at 55° N, the best possible choice. The damping timescale λ is 1/18 days at 55°. Also as with the SAM, the correlation of the AR1 model is somewhat improved (to 0.71) if we use mass fluxes through *both* 55° and 30° as inputs.

5. LAG-CORRELATIONS, CAUSALITY, AND MUTUAL FEEDBACKS

Our model explains a substantial portion of annular mode variability as an integrated response to PV flux forcing. But several authors (*Hartmann*, 1995; *Robinson*, 1991; *Lorenz and Hartmann*, 2001, 2003) discuss the feedback of annular mode variability onto synoptic eddy activity, leading to a mutual interaction between synoptic PV fluxes (QV) and annular mode index (AM). Our model certainly doesn't rule this out, since it is driven by observed PV fluxes which could include feedback processes within them, but we're focusing our attention only on the QV→AM part of the story. Our model is blind to the possibility of an AM→QV feedback, though it still suffices to describe QV→AM forcing even if feedback exists.

Can we detect such a feedback in the data? Is it a major factor?

To answer this, we compute the lag-autocorrelation of the PV flux forcing ($R_{QV,QV}$) and the annular mode index ($R_{AM,AM}$), and the lag-cross-correlation between the two ($R_{QV,AM}$). If QV is essentially white, that is, $R_{QV,QV}(\tau) = 0$ for lag $\tau \neq 0$, then our autoregressive model predicts that $R_{QV,AM} = 0$ when AM leads QV: that is, that a change in the annular mode does not feed back to cause a change in the PV flux. We expect a strong correlation when QV leads AM.

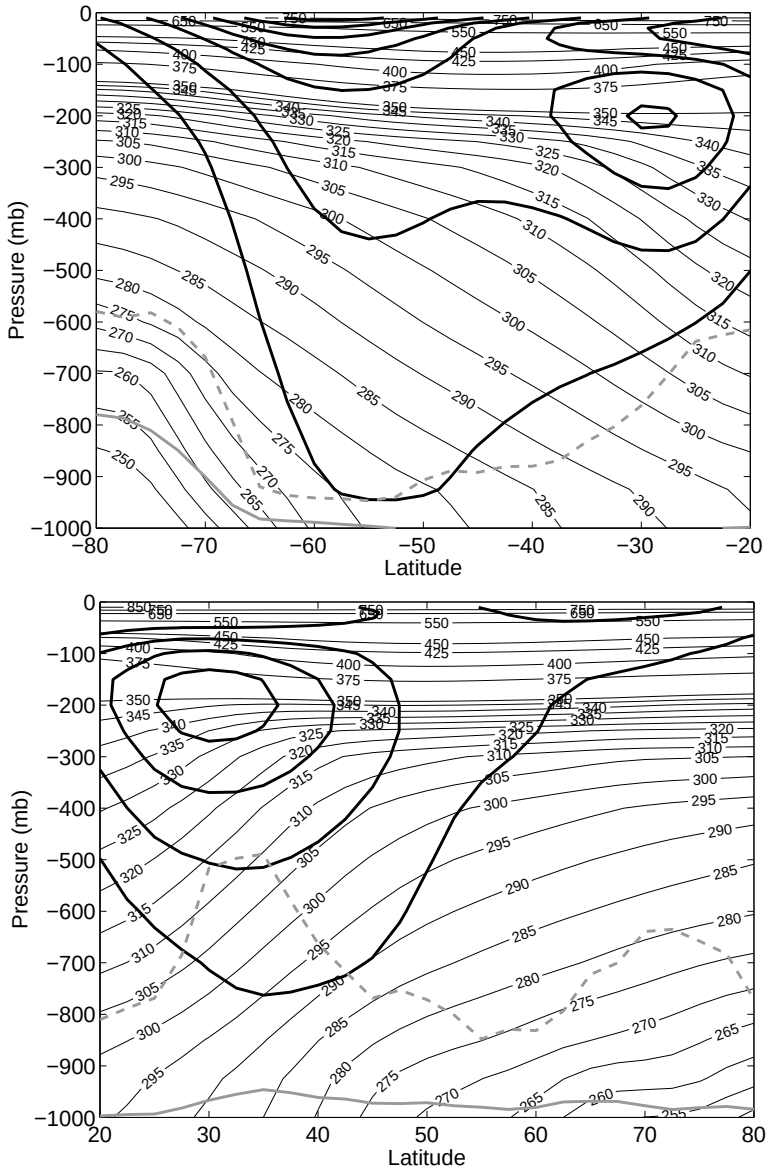

Figure 6. Isentropic layers used to compute meridional mass fluxes (zonally averaged θ in K, thin black lines). Also shown are the time and zonal mean (continuous gray) surface pressure (continuous gray), the minimum surface pressure encountered in the mean at each latitude (dashed gray line) and the zonally averaged zonal wind (heavy black lines, contour interval 10 m/s). Top: Southern hemisphere, Dec 2002-Feb 2003. Bottom: Northern hemisphere, June-August 2003.

One advantage to our 'reservoir model' approach is that it allows us to select good variables for this analysis. Of all the possible PV fluxes that might be influenced by the annular mode, it makes sense to select the fluxes occurring along the reservoir boundary line, which is the latitude where the AR model optimally captures the QV→AM forcing (See Figures 5, 7, etc.) In the analysis below, we project the QV forcing at all levels onto the $\mathbf{b}$ vector at that latitude to generate a single timeseries which picks out the QV forcing which is most important to annular mode excitation: annular mode feedbacks onto this particular variable will be most interesting and relevant.

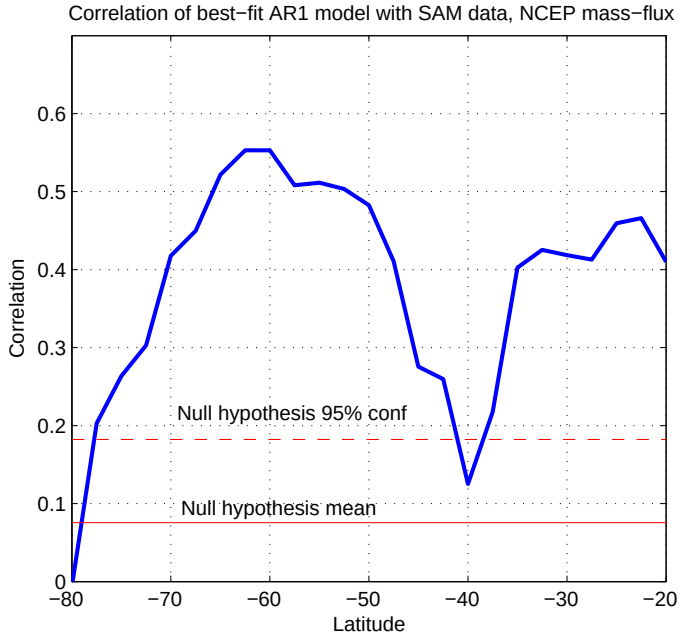

Figure 7. Same as 5, but for the NCEP-NCAR southern annular mode (SAM). Autoregressive model is driven by isentropic mass flux through a chosen latitude.

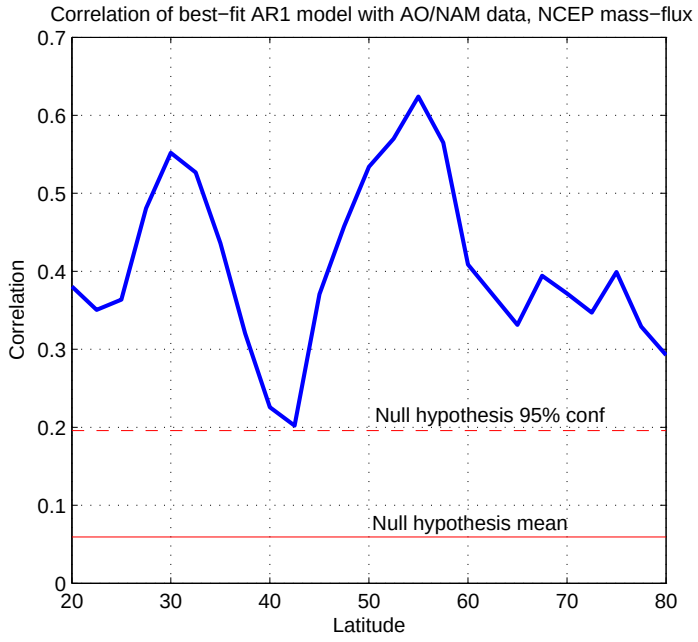

Figure 8. Same as 7, but for the northern annular mode (NAM/AO).

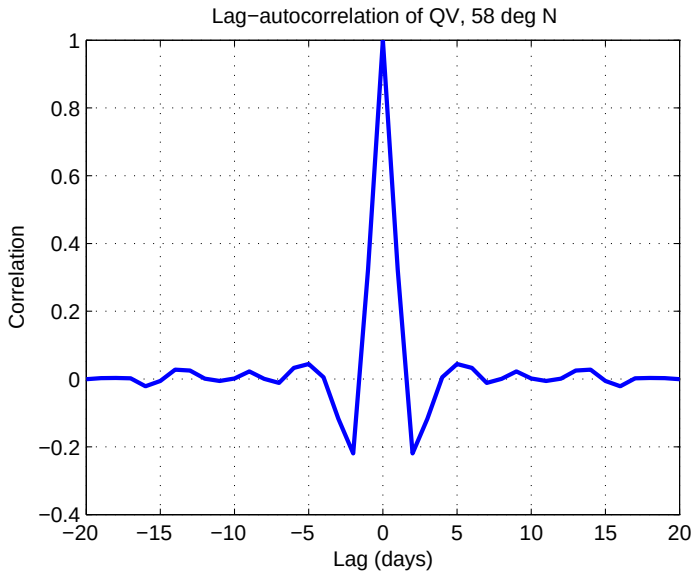

Figure 9. Lag-autocorrelation $R_{QV,QV}$ of PV flux (**b**·QV) at 58° for the 3-layer QG model.

(*a*) *3-layer QG Model*

The PV flux timeseries for the 3-layer QG model is essentially white for timescales longer than 5 days so (Figure 9). There is a significant negative correlation for lags of a few days: this is comparable to the duration of baroclinic waves, and may indicate weak wavelike periodicity of synoptic activity. Lag-autocorrelations for individual levels (not shown) show the same feature.

The mNAM index (Figure 10) is, as expected, strongly autocorrelated. The autocorrelation pattern $R_{mNAM,mNAM}$ is consistent with an exponential decay timescale of 37 days. This is intermediate between the best AR1 model damping timescale fits at 58° (31 days) and 25° (54 days), previously identified as areas of peak sensitivity. There's a small departure from exponential decay at lags of a few days, at the lag where the lag-correlation of the input PV flux forcing becomes negative.

The cross-correlation $R_{QV,mNAM}$ between PV flux and mNAM (Figure 11) is very interesting. At the 200 and 500 mbar levels, correlation is zero when mNAM leads QV: this is consistent with zero mNAM→QV feedback. At the lowest level (800 mbar) however, we see a strong positive feedback of the mNAM back onto the PV flux. Presumably this occurs because changing the amount of PV in the "reservoir" affects the amount of synoptic activity excited along its boundary, but it's unclear why this effect is limited to the lowermost model layer.

(*b*) *NCEP-NCAR Reanalysis Data*

Next, we consider the same analysis for the NCEP-NCAR data. We will focus attention on the NAM/AO mode; the SAM mode will be briefly considered. In all cases, the "mass flux" timeseries $MF(t)$ is the projection of the mass-flux data onto the AR1 model's optimal **b** vector at the latitude where the AR1 model is most effective at explaining the annular mode timeseries (62° S and 55° N for the SAM and NAM/AO, respectively). Thus, we're looking for feedbacks from the annular mode onto the mass flux at the location where the mass flux most effectively excites the annular mode.

Similarly to the 3-layer QG model, the isentropic mass flux shows rapid decorrelation, with a hint of a negative lag-correlation for short lags (a week, in this case) and no other structure. The AO index has a longer decorrelation time, about 6 days (Figure 13, broken curve), which is shorter than the exponential decay time computed for the AR1 model (18 days). It might be that the slow AR1 process only explains *part* of the AO variability – the unexplained processes mostly have shorter timescales. In particular, by making the long-wave approximation in using thickness flux as a proxy for PV flux, we may be selecting for the longer, slower modes.

Like the QG model, The AO analysis shows some correlation when AO leads mass flux, which is indicative of a AO→ mass flux feedback (Figure 14). But for reasons that remain unclear at present, this feedback is negative instead of positive, as indicated by the change in the sign of the cross-correlation function between positive and negative lags. It could be that the feedback present in the NCEP/NCAR data is not correctly represented in the 3-layer QG model. As discussed further in section 6(*c*), the feedback between the PV of the polar pool and the meridional PV flux at its equatorward edge seems to influence the autoregressive damping timescale found in our analysis.

The mass flux and annular mode index autocorrelations for the southern hemisphere (not shown) show very similar structure to the northern hemisphere. However, the lag-correlation diagram (Figure 15) shows no sign of a SAM→mass-flux feedback (correlation is zero when SAM leads mass flux. Thus, whatever feedback is occuring in the north seems not to be significant in the southern hemisphere.

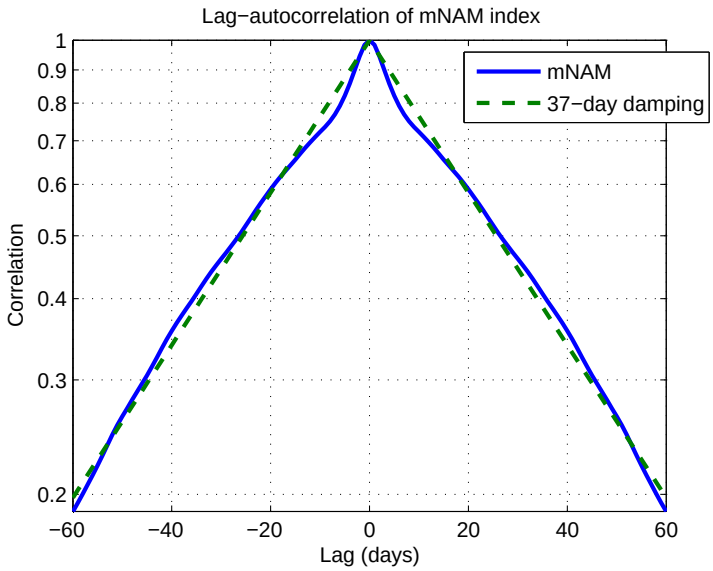

Figure 10. Lag-autocorrelation of mNAM index for the 3-layer QG model.

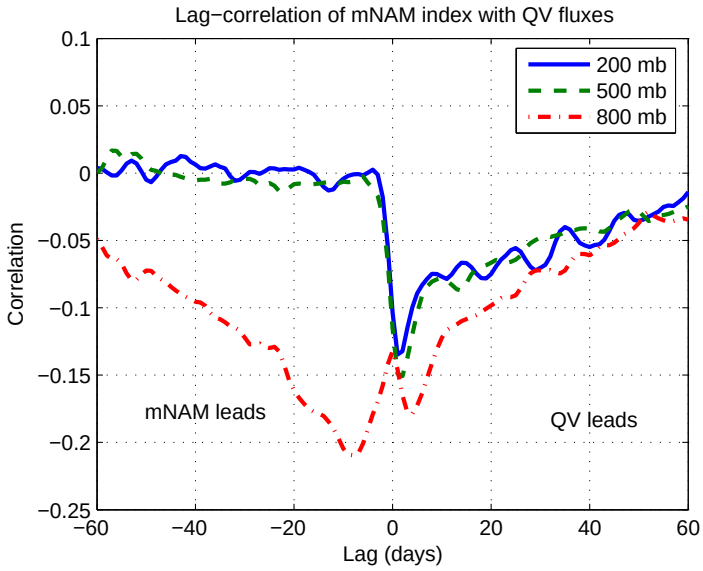

Figure 11. Lag cross-correlation between mNAM index and PV flux at 58° and at each level, for the 3-layer QG model.

6. Tangential Issues and Future Work

(*a*) *Spatial Structure of Annular Modes*

The model we consider helps to understand the time-variability of the annular modes, but can it explain their patterns? Why, for example, do both northern and southern annular modes have a zero-contour for pressure and PV anomalies at about 55-60°? Why not 40 or 70?

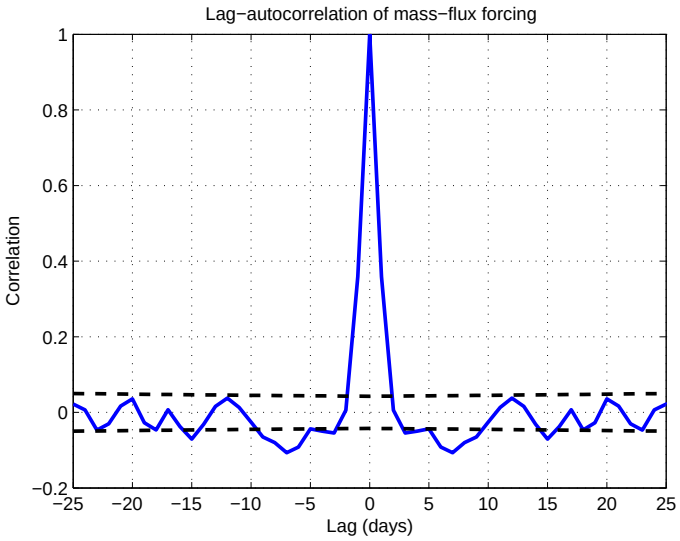

Figure 12. Lag autocorrelation $R_{MF,MF}$ of isentropic mass flux across 55° N, for NCEP-NCAR data. Dot-dashed line: expected lag-correlation for exponential decay with 6-day timescale. Dashed line: 95% confidence limit.

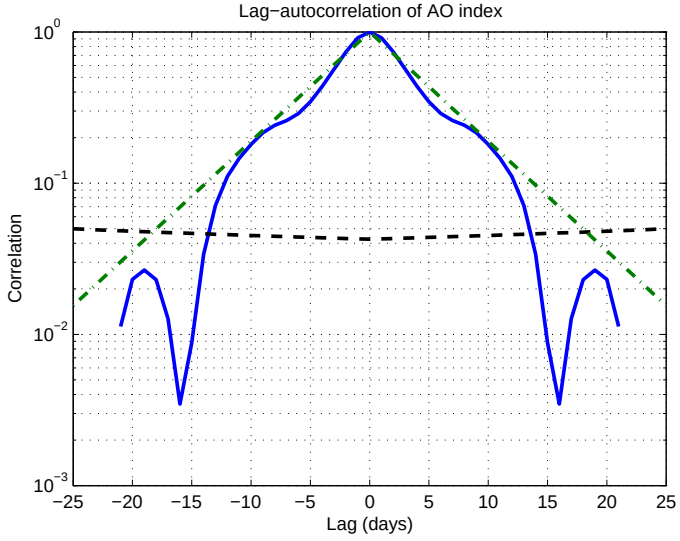

Figure 13. Lag autocorrelation $R_{AO,AO}$ of AO index for NCEP-NCAR data. Dashed lines: 95% confidence interval.

If stochastic PV/mass fluxes (which we argue play a key role in driving AM variability) had a maximum at 55-60°, we might have a partial explanation for the shape of the annular modes: the atmosphere might not be unusually sensitive to fluxes at this location, it's just that the flux variations are strongest there. Perhaps the pattern of the annular modes is set by the pattern of eddy PV flux variance. This idea was suggested (in terms of zonal momentum flux) by *Vallis et al.* (2004).

However, in fact, PV fluxes in the 3-layer QG model, and isentropic mass fluxes in NCAR-NCEP data for both hemispheres (not shown), show a peak in flux variance between 40 and 50°, a location well-known as the "storm track" latitudes. The peak sensitivity of our AR model is well north of the storm track, and nearly zero at the storm track location. In addition, if the hypothesis were correct, the AM would have PV anomalies north and south of the storm track latitude, and zero anomaly at the storm track. Figure 1 shows precisely

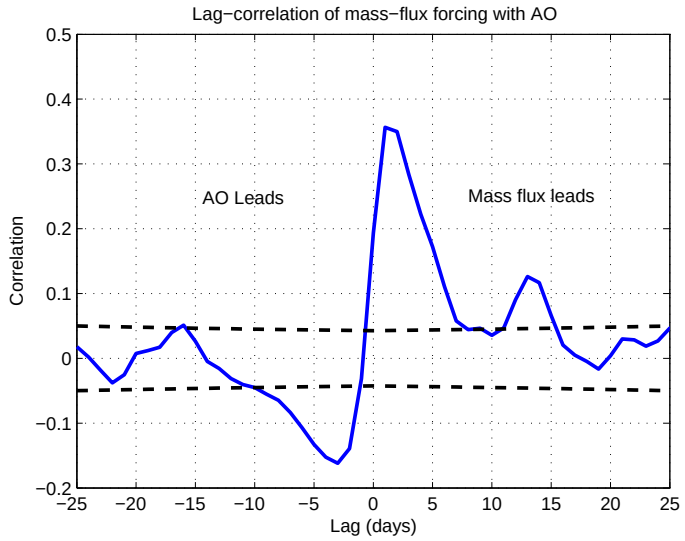

Figure 14. Lag cross-correlation $R_{MF,AO}$ of isentropic mass flux across 55° N with AO index, for NCEP-NCAR data. Dashed lines: 95% confidence interval. Note the change of sign compared with Figure 11 since the thickness flux and PV flux have opposite sign.

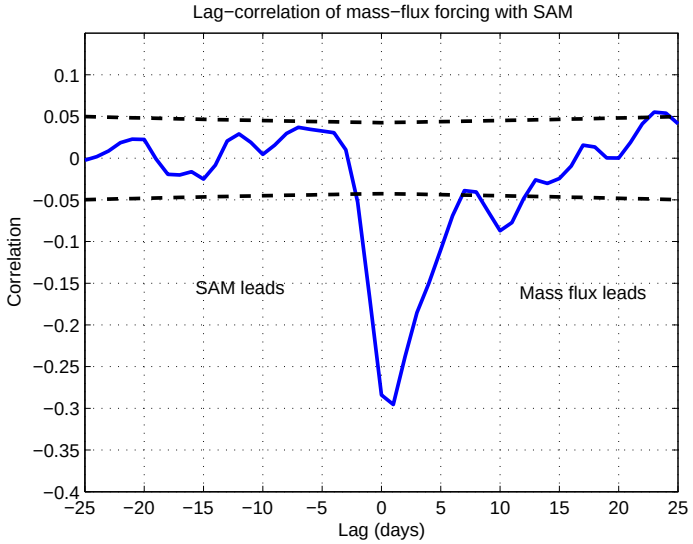

Figure 15. Lag cross-correlation $R_{MF,SAM}$ of isentropic mass flux across 62° S with SAM index, for NCEP-NCAR data. Dashed lines: 95% confidence interval. Note the change of sign compared with Figure 14 because of the change in the sign of the Coriolis parameter between Northern and Southern Hemispheres.

the opposite. Thus, the annular modes' shape is not strictly a consequence of the location of the PV fluxes which drive them, and indeed represent some "preferred mode" of the system. See *Goodman and Marshall* (2002) for ideas about the dynamics that might set up these modes.

An alternative explanation might lie in thinking not about a fixed storm track but in thinking about a meridionally shifting storm track. The location of the PV pools would then be set by the most poleward and equatorward latitudes spanned by the storm track while it

T_d	$1/\lambda$
18 days	48 days
25 days	31 days
36 days	28 days

TABLE 1. 3-layer QG model thermal dissipation timescale T_d compared with lag-correlation parameter λ for a best-fit AR1 model relating PV flux through 58° N with mNAM index.

shifts. A 10° shifts of the storm track seems sufficient to explain the $50^\circ - 60^\circ$ boundary of the polar PV pool. Whether these shifts are coupled or not to the PV pool is an open issue at that stage.

(*b*) *Damping Timescales*

One of the most useful products of our analysis is an estimate of the decay timescale of reservoir PV anomalies (λ). What determines this decay time?

For both the 3-layer model and real-world analyzed fields, the decay timescales are on the order of 3-4 weeks. This is not far from the radiative damping timescale for many parts of the atmosphere, leading to the hypothesis that PV anomalies in the reservoirs dissipate as their associated temperature anomalies decay.

For the NCEP-NCAR data, one can only speculate, but with the 3-layer QG model, one can actually change the thermal decay timescale in the model and see what happens. By default, the radiative damping time is 25 days, but it can be varied between 18 and 36 days without losing numerical stability. We performed the analysis of Section 4(*a*) twice more with thermal damping timescale $T_d = 18$ days and 36 days. The basic PV forcing field, bottom-drag timescales, and other parameters remained the same; only T_d was changed.

The time-mean flow field changes in strength, but in both of these extremes the first EOF pattern remains a slightly modified but clear North Annular Mode. The AR1 analysis gives remarkably similar results to the default case (in particular, the goodness-of-fit plots for the AR1 models (see Figure 5) are almost unchanged.

The only parameter that is consistently different is the reservoir damping timescale λ^{-1} (See Table 1), but the relationship is the opposite of what one might expect: when T_d is long, λ^{-1} is short and vice versa! The annular mode timescale is not simply given by the thermal damping timescale, disproving our hypothesis. The reason for the inverse relationship remains mysterious, and will be investigated in future work.

(*c*) *NAM vs SAM*

Previous authors (*Thompson and Wallace*, 2000a), (*Baldwin*, 2001) have remarked on the similarity between the NAM and SAM patterns, especially when considered in a zonal-average sense. Our analysis supports this, to a certain extent: the annular mode is strongly responsive to synoptic fluxes through roughly 30° and 60° latitude in both hemispheres. However, we also find some interesting differences. The NAM has a shorter autoregressive damping timescale (1/18 days, compared to 1/28 days for the SAM). The NAM also shows a negative feedback from the mode index onto the synoptic fluxes, whereas the SAM does not (Section 5(*b*)). Could these two effects be linked? The negative feedback in the NAM would act as an extra damping effect on the NAM which is not present in the SAM. The results from the 3-layer QG model support this idea: there, we find a *positive* mNAM→flux feedback, which corresponds to a longer λ timescale than either of the NCEP/NCAR modes.

7. CONCLUSIONS

We have demonstrated that a rather simple mechanism can explain a large amount of the variability of the annular modes in both northern and southern hemispheres. The annular modes are described as “reservoirs” of potential vorticity over the poles, each with a companion reservoir in middle latitudes. Synoptic weather events shuttle potential vorticity back and forth across the boundary between midlatitude and polar reservoirs; a small damping term tends to eliminate PV anomalies. This can be described using a simple autoregressive model.

In Figure 16, we present a cartoon analogy for this mechanism. We visualize the annular mode as a pair of tanks representing two reservoirs (the pole and the subtropics). The tanks contain some amount of water (PV), and are connected by a pump (synoptic weather). The pump turns randomly in either direction, moving PV back and forth between the tanks.

The storage of PV in the two reservoirs allows the annular mode to persist in one state for weeks or months, much longer than the daily timescales of the input weather forcing. However, this persistence time appears to be inversely related to the thermal damping time in our QG model, for reasons which remain unexplained.

While this view only describes the response of the annular mode to synoptic forcing, we find that a smaller feedback of the annular mode onto the synoptic variability does exist, and may affect the persistence timescales of the annular mode. While northern and southern hemispheres display similar ”reservoir” behavior, their feedbacks and timescales differ, for reasons which are not yet understood and require further study.

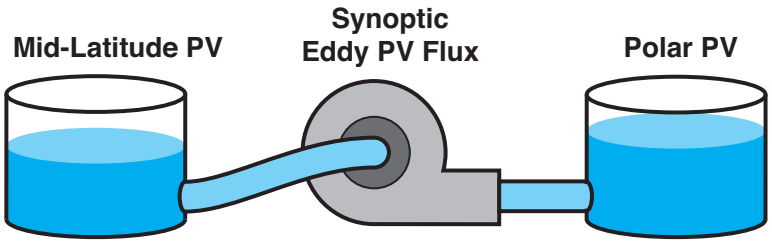

Figure 16. Cartoon analogy for our annular mode forcing mechanism. See Section 7 for details.

REFERENCES

Baldwin, M. P. 2001 Annular modes in global daily surface pressure. *Geophysical Research Letters 28*, 4115–4118.

Feldstein, S. B. 2000 The timescale, power spectra, and climate noise properties of teleconnection patterns. *Journal of Climate 13*, 4430–4440.

Gill, A. E. 1982 *Atmosphere–Ocean Dynamics*. Academic Press.

Goodman, J. C., and J. Marshall 2002 Using neutral singular vectors to study low-frequency atmospheric variability. *J. Atmospheric Sciences 59*, 3206–3222.

Goodman, J. C., and J. Marshall 2003 The role of neutral singular vectors in midlatitude air-sea coupling. *J. Climate 16*, 88–102.

Hartmann, D. L. 1995 A PV view of zonal flow vacillation. *Journal of the Atmospheric Sciences 52*, 2561–2576.

Held, I. M., and T. Schneider 1999 The surface branch of the zonally averaged mass transport circulation in the troposphere. *Journal of the Atmospheric Sciences 56*, 16881697.

Kalnay, E. M., et al. 1996 The NCEP/NCAR reanalysis project. *Bulletin of the American Meteorological Society 77*, 437–471.

Lorenz, D. J., and D. L. Hartmann 2001 Eddy–zonal flow feedback in the Southern Hemisphere. *Journal of the Atmospheric Sciences 58*, 3312–3327.

Lorenz, D. J., and D. L. Hartmann 2003 Eddy–zonal flow feedback in the Northern Hemisphere winter. *Journal of Climate 16*, 1212–1227.

Molteni, F. 1994 Towards a dynamical understanding of planetary-scale flow regimes, Ph.D. thesis, Imperial College, University of London.

Namias, J. 1950 The index cycle and its role in the general circulation. *Journal of Meteorology 7*, 130–139.

North, G. R. 1984 Empirical orthogonal functions and normal-modes. *J. Atmos. Sci. 41*, 879–887.

Robinson, W. A. 1991 The dynamics of the zonal index in a simple model of the atmosphere. *Tellus 43A*.

Rossby, C. G., and H. C. Willett 1948 The circulation of the upper troposphere and lower stratosphere. *Science 108*, 643–652.

Thompson, D. W., S. Lee, and M. P. Baldwin 2003 *The North Atlantic Oscillation: Climatic Significance and Environmental Impact*. vol. 134 of *Geophysical Monograph Series*, chap. Atmospheric Processes Governing the Northern Hemisphere Annular Mode/North Atlantic Oscillation, pp. 81–112, American Geophysical Union.

Thompson, D. W. J., and J. M. Wallace 2000a Annular modes in the extratropical circulation. Part i: Month-to-month variability. *Journal of Climate 13*, 1000–1016.

Thompson, D. W. J., and J. M. Wallace 2000b Annular modes in the extratropical circulation. Part ii: Trends. *Journal of Climate 13*, 1018–1036.

Vallis, G. K., E. P. Gerber, P. J. Kushner, and B. A. Cash 2004 A mechanism and simple dynamical model of the North Atlantic Oscillation and annular modes. *Journal of the Atmospheric Sciences 61*, 264–280.